The Astronomical Journal, 126:2971–2987, 2003 December

INVESTIGATION OF 131 HERBIG Ae/Be CANDIDATE STARS[1]

S. L. A. Vieira,[2] W. J. B. Corradi,[2] S. H. P. Alencar,[2,3] L. T. S. Mendes,[2]
C. A. O. Torres,[4] G. R. Quast,[4] M. M. Guimarães,[2] and L. da Silva[5]
Received 2002 August 19; accepted 2003 August 29

ABSTRACT

We present a new catalog of 108 Herbig Ae/Be candidate stars identified in the Pico dos Dias Survey, together with 19 previously known candidates and four objects selected from the *IRAS* Faint Source Catalog. These 131 stars were observed with low- and/or medium-resolution spectroscopy, and we complement these data with high-resolution spectra of 39 stars. The objects present a great variety of Hα line profiles and were separated according to them. Our study suggests that most of the time a Herbig Ae/Be star will present a double peak Hα line profile. Correlations among different physical parameters, such as spectral type and $v \sin i$ with Hα line profiles were searched. We found no correlation among Hα line profiles and spectral type or $v \sin i$ except for stars with P Cygni profiles, where there is a correlation with $v \sin i$. We also use preliminary spectral energy distributions to seek for any influence of the circumstellar medium in the Hα line profiles. The presence of [O i] and [S ii] forbidden lines is used together with the Hα line profiles and these preliminary spectral energy distributions to discuss the circumstellar environment of the Herbig Ae/Be candidates. The distribution of the detected [O i] and [S ii] forbidden lines among different spectral types points to a significantly higher occurrence of these lines among B stars, whereas the distribution among different Hα profile types indicates that forbidden lines are evenly distributed among each Hα line-profile type. Combining the distance estimates of the Herbig candidates with the knowledge of the interstellar medium distribution, we have found that 84 candidates can be associated with some of the more conspicuous SFRs, being in the right direction and at a compatible distance. As a further means of checking the properties of the HAeBe candidates, as well as their present evolutionary status, the derived luminosities and effective temperatures of the stars with possible association to the star-forming regions and/or *Hipparcos* distances were plotted together with a set of pre–main-sequence evolutionary tracks on an HR diagram. A set of 14 stars were found out of their expected positions in the HR diagram.

Key words: catalogs — circumstellar matter — ISM: clouds — stars: pre–main-sequence — techniques: spectroscopic

1. INTRODUCTION

Determining whether a star belongs to the Herbig Ae/Be (HAeBe) group or not has been a topic of great discussion, with various criteria being used in the literature for the classification. In general, to be undoubtedly considered an HAeBe star, a candidate should present the following characteristics:

1. spectral type A or earlier, with emission lines;
2. located in an obscured region;
3. fairly bright nebulosity in its immediate vicinity;
4. present an anomalous extinction law;
5. show infrared excess;
6. be photometrically variable; and
7. display line profiles of Mg ii (λ2800) in emission.

The first three criteria were proposed by Herbig (1960) to define pre–main-sequence (PMS) stars of intermediate mass. The last four are an extension proposed by Thé et al. (1994, hereafter TWP) to encompass the large set of new candidates. However, very few stars satisfy all of them. One possible explanation is that the HAeBe group spans a large range of evolutionary stages (Malfait et al. 1998).

A feature common to all HAeBe objects is the presence of infrared excess due to thermal reradiation, usually explained by the presence of an accretion disk or an almost symmetric circumstellar halo. Malfait et al. (1998) proposed different envelope shapes based on the spectral energy distributions (SEDs) obtained for 45 HAeBe stars. Imhoff (1994) found a correlation between the UV Mg ii line profile and infrared excess. All the stars in his sample with strong near-infrared excess showed the Mg ii line with P Cyg (indicator of winds) or double-peaked profiles (winds or disks), while those with weak IR excess presented the Mg ii line in absorption.

Forbidden lines such as [O i] (λ6300 and λ6364) and [S ii] (λ6716/λ6731) trace the emission from low-density regions near the stars. The shape of the forbidden-line profiles can indicate the presence of disks or outflow characteristics. When a disk exists, these lines are expected to be blueshifted and asymmetric, as in T Tauri stars (TTSs) (Finkenzeller 1985), since the receding part of the outflow will be hidden by the disk. In HAeBe stars there is still a debate on the origin of the observed forbidden lines. Almost all observed [O i] lines are symmetric, and some authors (e.g., Böhm & Catala 1994; Böhm & Hirth 1997) favor the idea of an origin in a spherically symmetric wind without the presence of disks. Others, in contrast, (Corcoran & Ray 1997) suggest

[1] Based on observations made at the Obsevatório do Pico dos Dias/LNA (Brazil), ESO (Chile), and the Lick Observatory.

[2] Departamento de Física, ICEx, Universidade Federal de Minas Gerais, C.P. 702, 30161-970 Belo Horizonte, MG, Brazil; slvieira@fisica.ufmg.br, wag@fisica.ufmg.br, silvia@fisica.ufmg.br, luizt@fisica.ufmg.br, mmg@fisica.ufmg.br.

[3] Universidade de São Paulo, IAG, Departamento de Astronomia, Rua do Matão 1226, Cidade Universitária, 05508-900 São Paulo, Brazil.

[4] Laboratório Nacional de Astrofísica, MCT, Rua Estados Unidos 154, 37504-364 Itajubá, Brasil; beto@lna.br germano@lna.br.

[5] Observatório Nacional, MCT, Rua General José Cristino 77, 20921-400 São Cristóvão, Rio de Janeiro, Brazil; licio@on.br.

that these lines come from winds originating in the outermost parts of a disk, since the forbidden lines are very narrow compared with the typical stellar wind velocity of hundreds of kilometers per second inferred from P Cyg profiles of permitted lines.

The presence of disks around HAeBe stars can be probed by simultaneous photometric and spectroscopic observations. Grinin et al. (1994) and Vieira et al. (1999) observed Algol-like minima accompanied by variations in the Hα profile of UX Ori and HD 100546, which can be explained by inhomogeneities or clumps orbiting the star in an edge-on disk. Nowadays, a few HAeBe stars, including HD 100546, have had their disks directly imaged with coronographic techniques (Augereau et al. 2001; Mouillet et al. 2001).

The aim of this work is to present a statistical analysis of a sample of 131 HAeBe stars for which we have low- and medium-resolution spectra, covering the spectral range 4300–6800 Å.[6] For most of them (107) we also have nonsimultaneous *UBVRI* photometry, which is used to obtain physical parameters.

2. DATA SELECTION

Using the *IRAS* Point Source Catalog, a search for new TTSs was conducted at the Observatório do Pico dos Dias (operated by the Laboratório Nacional de Astrofísica/MCT, Brazil), the so-called Pico dos Dias Survey (PDS) (Gregorio-Hetem et al. 1992; Torres et al. 1995; Torres 1999). The candidate stars were selected by searching for starlike objects brighter than 14 mag (eye estimated) in the images of the Digitized Sky Survey within 3.3 σ of the *IRAS* position errors, south of 30° north and possibly associated with sources having infrared fluxes with spectral indices in the interval

$$-1.35 \leq \alpha_1 \leq 2.0 , \quad (1)$$

$$-1.85 \leq \alpha_2 \leq 1.5 . \quad (2)$$

The indices were defined as follows:

$$\alpha_1 = 3.14 \times \log(F_{25}/F_{12}) - 1 , \quad (3)$$

$$\alpha_2 = 2.63 \times \log(F_{60}/F_{12}) - 1 , \quad (4)$$

where F_{12}, F_{25}, and F_{60} are fluxes in the infrared at 12, 25, and 60 μm, respectively. Known QSOs, active galactic nuclei, and planetary nebulae were rejected, as well as stars in the Herbig & Bell Catalog (Herbig & Bell 1995, hereafter HBC).

Since our search for TTSs using *IRAS* colors was based on dust properties and not on the star itself, our selection criteria also included HAeBe stars. It is more difficult to be certain of the classification of a HAeBe star than of a TTS, because there is no feature like the Li (λ6707) line as a clear signature of this class of objects. We used the following criteria to extract the HAeBe candidate objects:

1. stars that present spectral type earlier than F5 with emission in Hα, and
2. Hα that does not seem to come from the circumstellar nebula, and
3. objects that are not supergiants, symbiotics, or LBVs, and
4. objects that have the spectral index $\beta \gtrsim -2$.

The β index is defined as $\beta = 0.75 \log(F_{12}/F_V) - 1$, where F_V is the flux in the visual band. This last condition allows to eliminate weaker infrared sources as classical Be or Vega-like stars.

Using these criteria, the PDS identified 105 HAeBe candidate stars (three being HAeBe binaries), but actually only 92 brighter than 14 mag.

The main previous compilations of HAeBe stars are HBC and TWP. In the HBC, using the first of the above criteria to define HAeBe stars, there are 71 candidates. In TWP there are 108 candidates (in their first table), 63 in common with HBC. Excluding three stars from the list of TWP that seem to be misclassified, the HBC+TWP forms a sample of 113 "known" HAeBe candidates. From these stars, only 41 obey the PDS magnitude, declination, and spectral index limits. Due to its long duration, 18 stars of the PDS were also proposed as HAeBe candidates by TWP (by definition, none are part of the HBC), and all of the other 23 stars are both in HBC and TWP. Thus the "complete" sample within the PDS limits would be of 115 stars (92 from PDS plus 23 from HBC).

Actually, this is not a truly complete sample, first because of the variations in magnitude and Hα emission that could

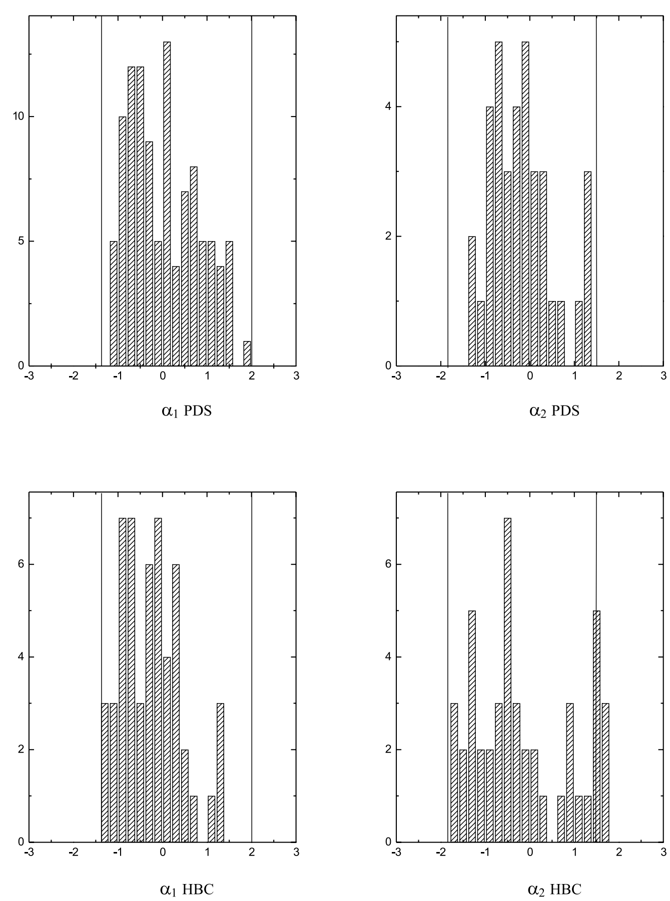

FIG. 1.—Histograms showing distribution of HAeBe candidates from PDS (*top*) and HBC (*bottom*) according to spectral indices α_1 and α_2.

[6] The low- and medium-resolution spectra are available for download at http://www.fisica.ufmg.br/~svieira/TRANSF.

TABLE 1

Log of Spectroscopic Observations of Herbig Ae/Be Candidate Stars

PDS (1)	Name (2)	*IRAS* (3)	S. R. (4)	Sp. Type (5)	Type (6)	F. L. (7)
002	CD-53 251	01156−5249	M	F3 V	I	–
004	GSC 1811−0767	03359+2932	M	A0	I	[O I]
168	GSC 1829−0331	04278+2253	M	F1	I	–
	HBC 078	04525+3028	M, H	B9	IV	[O I]
172^{T}	HD 31648	04555+2946	M, H	A3 V	IV	[O I]
174	A0974-15	05044−0325	L, M	B3	II	–
176^{T}	HD 34282	05136−0951	L, M	A0	II	–
178N	HD 35187N	05209+2454	L, M	A0 V	I	–
178S	HD 35187S	05209+2454	L, M	A7 V	?	–
179	HD 287823	05215+0225	L, M, H	A0	IV	–
180^{T}	HD 287841	05221+0141	L, M	A8 V	II?	–
114	HD 290409	05245+0022	L, M	B9	II	–
QT1	HD 290500	F05272−0025	M	A2	III	–
183^{T}	HD 36112	05273+2517	M, H	A8 V	I	[O I]
184	HD 244314	05275+1118	M	A1 V	I	–
185S	HD 36408	05293+1701	M, H	B8	abs	–
187	UY Ori	05295−0458	L, M, H	B9	III	[O I]+[S II]
190	HD 290770	05345−0139	L, M, H	B9	II	[O I]+[S II]
191^{T}	HD 37357	05353−0644	L, M, H	A1 V	IV	–
192	HD 290764	05355−0117	L, M	F0 V	I	–
193^{T}	GSC 4779−0040	05357−0650	L, M	A5	II	–
194^{T}	HD 37411	05357−0526	M	B9	II	–
198^{T}	V599 Ori	05365−0718	M	F0	II	–
016	HD 38120	05407−0501	M, H	B9	I	[O I]
201	V351 Ori	05417+0007	M	A7 V	III?	–
204	MWC 778	05471+2351	M	B1?	II	[O I]+[S II]
018	GSC 5352−0159	05513−1024	M	B7?	II	[O I]+[S II]
019	GSC 5360−1033	05555−1405	M	B5?	II	?
020	HD 249879	05560+1639	M, H	B8?	I	[O I]
021	AS 116	05598−1000	L, M, H	B5?	IV	[O I]
022	AS 117	06013−1452	L, M, H	A0	I	[O I]
207	GSC 1876−0892	06040+2958	M	B2	II	–
124	GSC 4794−0827	06045−0554	M, H	A0	I	[O I]
211		06071+2925	M	B9	I	[O I]
126	GSC 4795−0492	06111−0624	M	A7 V	III	–
216	CPM 25	06210+1432	M	B2	II	[O I]
023	NSV 2968	06245−1013	M	B0	IV	[O I]+[S II]
024	GSC 5950−0021	06464−1644	L, M	B9	II	[O I]
130	GSC 5379−0359	06475−0735	L, M	B9	IV	–
225	HD 50083	06491+0508	L, M, H	B3	III	–
025	NSV 3275	06523−2458	M	A3	II	–
229N	GSC 4805−1872	06531−0305	M	A0	IV	–
234	GSC 4805−1306	06562−0337	M	O9?	II	[O I]+[S II]
	HD 52721	06594−1113	M	B2 Vn	II	–
	HBC 548	07003−1121	M, H	A	III	[O I]+[S II]
	HBC 551	07017−1121	M, H	B5	III	[S II]
	HD 53367	07020−1022	M, H	B4	II	–
286	Hen 3-248	09042−4706	L, M	B0 V	I	–
290	GSC 8584−2884	09245−5228	M	B7	?	–
297	GSC 8593−2802	09410−5601	L	A7?	II?	–
	HD 85567	09489−6044	M	B9	I	[O I]
303	HD 87403	10012−5902	M, H	A1	II?	–
037	Hen 3-373	10082−5647	L	B2?	III	–
315	HD 305298	10312−6004	L, M	O8	IV	–
322N	GSC 8618−2363	10501−5556	M	B3	?	–
324		10554−6237	L	B1?	II?	–
	HD 95881	11002−7114	L, M	A0	II	[O I]*
327	HD 96042	11016−5910	M	B1	II	[O I]+[S II]
	HD 98922	11202−5305	L, M	B9	IV	[O I]
339	HD 100453	11307−5402	L, M, H	A9 V	III	–
340^{T}	HD 100546	11312−6955	L, M, H	B9 V	III	[O I]
057^{T}	HD 101412	11373−5953	L, M, H	A0	II	[O I]
344	VdBH 52	11382−6415	L, M	B5?	II	–
139		11507−6148	L	B0	III	–
061^{T}	HD 104237	11575−7754	L, M	A0+Sh	III	–
140	GSC 8645−1401	12150−5927	L, M	F2	IV	–
353	Hen 2-80	12196−6300	L, M	B5?	II	[O I]+[S II]
141^{T}	DK Cha	12496−7650	M	A?	II?	?
	Hen 3-847	12584−4837	L, M	B5	I	[O I]+[S II]
361	GSC 8993−0397	13002−6157	L, M	B3	II	–
QT4	HD 114981	F13118−3823	L	B5 V	II	–
364	WRAY 15-1090	13168−6208	L, M	B2	II	–
371N		13445−3624	M	O9?	I	[O I]+[S II]
067	Hen 3-938	13491−6318	L, M	O9?	III	[O I]
069N	Hen 3-949	13547−3944	L, M, H	B3	III	[O I]
	HBC 596	14592−6311	M	B	IV	–
389		15106−6205	L, M	A3 V	IV	–
394		15310−6149	M	F0 V	?	–
395	HD 139614	15373−4220	L, M, H	A8 V	I	–
144N		15462−2551	L, M	A2 IV	II	[O I]+[S II]
144S	CD-25 11111	15462−2551	M, H	A5 V	II	[O I]+[S II]
398A^{T}	HD 141569	15473−0346	L, M, H	A0 V	II	[O I]
399B		15504−5510	L, M	B2	I	[O I]+[S II]
399A	HD 141926	15504−5510	M, H	B2 IIIn	I	–
076^{T}	HD 142666	15537−2153	L, M, H	A8	II	[O I]
406	GSC 7855−0815	16017−3936	M	A5 V	II	[O I]
078^{T}	HD 144432	16038−2735	L, M, H	A8	IV	–
	HBC 619	16052−3858	L, M	A7	II	–
080	HD 145718	16102−2221	L, M, H	A8 IV	II	[O I]+[S II]
415N	CD-23 12840	16156−2358	L, H	F0 V	abs	–
	HD 150193	16372−2347	L, M	A0 V	IV	–
431		16513−4316	L	A0	II	–
453	GSC 6829−0106	17178−2600	L	F2 V	III	–
095	HD 319896	17277−3506	L, M	B4	I	–

TABLE 1—*Continued*

PDS (1)	Name (2)	*IRAS* (3)	S. R. (4)	Sp. Type (5)	Type (6)	F. L. (7)
241.........	GSC 4823−0146	07061−0414	M, H	B0	I	[O I]
027.........	DW CMa	07173−1733	M, H	B2?	IV	[O I]
	HBC 552	07178−4429	M	F+sh	II	[O I]
249.........	GSC 6546−3156	07222−2610	M	A0	I	–
250.........	GSC 6542−2339	07225−2428	M	O9?	III	[O I]+[S II]
133.........	SPH 6	07230−2539	M	B6	III	[O I]+[S II]
255.........	SS73 6	07296−1921	M	B1?	II	[O I]
134.........	SS 127	07303−2148	M	B6	II	–
257.........	GSC 5988−2257	07394−1953	M	B3	II	[O I]
QT2.......	GSC 8143−1225	F07577−5014	L	F3 V	?	–
272.........	HD 68695	08100−4356	L, M	A0 V	I	–
277.........	CD-38 4380	08213−3857	L, M	F3 V	I	–
031S.......	HD 72106S	08277−3826	M	A0	I	?
QT3.......	GSC 8581−2002	F08432−5945	L	A5 V	?	–
033.........	GSC 7679−0293	08469−4037	L, M	A0	II	–
034.........		08482−4541	L, M	B2	II	[O I]
	HD 76534N	08533−4316	M	B2	II	–
	HD 76534S	08533−4316	M	B3	II	–
281.........	SAO 220669	08539−4413	L	B4	II?	–

PDS (1)	Name (2)	*IRAS* (3)	S. R. (4)	Sp. Type (5)	Type (6)	F. L. (7)
096........	HD 323771	17306−3921	L, M	B5 Vp	IV	–
465........	Hen 3-1475	17423−1755	M	B7	III	[O I]
469........	GSC 5673−0127	17481−1415	M	A0	I	–
473[T]......	HD 163296	17533−2156	L, M, H	A0	II	[O I]+[S II]
477........		17575−1647	M	B1	III	[O I]
514........	HD 169142	18213−2948	L, M, H	A9	I	[O I]
518[T]......	MWC 297	18250−0351	M	B0	I	[O I]
	HBC 282	18262+0006	M	B+sh	II	[O I]
520........	GSC 0446−0153	18275+0040	M	F3 V	II	[O I]
530........		18391+0805	M	F0 V?	I	[O I]+[S II]
543........		18454+0250	M, H	B1	I	
545........	MWC 610	18483+0838	M, H	B2	II	–
551........		18528+0400	M	O9?	III	[O I]
	HBC 287	18583−3657	M	B9	?	–
	HBC 288	18585−3701	M	A0+sh	II	[O I]
564[T]......	HD 179218	19089+1542	M, H	A0 V	I	[O I]
581........	GSC 2150−0266	19343+2926	M, H	B0.5 IV	I	[O I]+[S II]
	HD 190073	20005+0535	M, H	A0 IVp+sh	IV	[O I]

NOTES.—The first column is the star identification in the PDS program, the T superscript identifying the PDS objects also proposed to be HAeBe by Thé et al. 1994. QT (from Quast and Torres) are used to identify the stars taken from the *IRAS* Faint Source Catalog. When available, another identification is presented in col. (2). Col. (3) has the *IRAS* identification and col. (4) has the spectral resolution: L for low, M for medium, and H for high; col. (5) has the spectral type classification by the PDS program. Col. (6) has the Hα line-profile classification according to Reipurth et al. 1996, the question mark means that the spectra quality is too poor to be classified, and "abs" means that the profile is in absorption. Col. (7) shows the presence of forbidden lines: [O I]* means that only 6300.31 Å is present; the question mark means that the spectra begin at 6500 Å and nothing can be said about the presence of the [O I] lines; the minus sign means that [O I] and [S II] forbidden lines are not present.

cause some loss of objects. Furthermore, a sample based on *IRAS* could not form a complete sample because of its incomplete and inhomogeneous sky coverage. Another problem may arise with the spectral index limits. As the *IRAS* spectral indices are optimized for a TTS search, we checked how they work for HAeBe using the 57 HBC HAeBe that have *IRAS* fluxes. In Figure 1 we show the histograms of both spectral indices of the PDS and HBC samples. For the HBC sample, considering the *IRAS* flux limits, we used stars that have at least one of the spectral indices defined. One can see that both samples have similar distributions for α_1, showing that the used limits are adequate. In the case of α_2 some HAeBe candidates may have been lost in PDS because their indices could be out of the limits (specially for the upper limit). But within the PDS criteria, the 115 stars form a nearly complete sample. It is important to note that our sample is less biased toward bright objects than other catalogs since we used *IRAS* colors (not limited by the source brightness) as selection criteria.

In the present paper we added to the 105 stars observed in the PDS (or 108, if each member of the binaries is counted) 19 stars that were previously identified as HAeBe candidates: 10 from TWP and nine from HBC. We also included four stars from the *IRAS* Faint Source Catalog, HD 290500, GSC 8143−1225, GSC 8581−2002, and HD 114981. Thus, we are presenting in this paper 131 HAeBe candidates.

The PDS and *IRAS* identifications, the spectral classification, and other information about the HAeBe candidates discussed in the following sections can be found in Table 1.

3. OBSERVATIONS

3.1. *Photometry*

Johnson $UBV(RI)_c$ measurements were gathered for 107 of the 131 stars in 63 nights during a period of 8 yr (1990–1998). The observations were collected at OPD (Brazil) with the 60 cm Zeiss telescope equipped with the FOTRAP photometer (Jablonsky et al. 1994). Standard stars were taken from Graham (1982), and the data were reduced using a package developed by Jablonsky et al. (1994). Further details of the reduction scheme can be found in Torres (1999).

Interstellar extinction was determined using the $B-V$ and $V-I$ colors, which are less affected by the presence of emission lines, and the calibrations of Schmidt-Kaler (1982) and Kenyon & Hartmann (1995) using spectral types determined as explained in the next section. Since our main goal is to have only indicative values, we used $R = 3.3 + 0.28(B-V)_0 + 0.04E_{(B-V)}$ (Schmidt-Kaler 1982) for all stars, independently of their position in the sky. The photometric data used and the derived parameters are listed in Table 2.

3.2. *Spectroscopy*

Low- and medium-resolution spectra of all the objects presented in Table 1 were used to carry out a statistical analysis of the features supposedly associated with the HAeBe class. Examples of such spectra are shown in Figure 2, covering the total observed wavelength range at each resolution (low: 4790–6880 Å and medium: 6290–6745 Å, except for three stars where the spectra start at 6500 Å). We also used high-resolution echelle spectra collected for 39 stars at ESO (Chile) and the Lick Observatory.

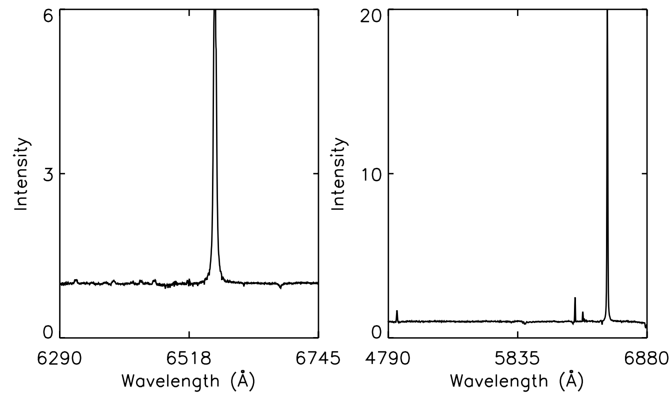

FIG. 2.—Medium-resolution spectrum of PDS 225 (*left*) and low-resolution spectrum of PDS 353 (*right*). Both spectra show the Hα line in emission.

The low-resolution spectra were collected with the Cassegrain spectrograph of the 1.6 m telescope at OPD, using a 1024 × 1024 pixel CCD and a diffraction grating of 600 lines mm^{-1}. The spectra have a signal-to-noise ratio (S/N) of ≈80, and a resolving power of $R = 1000$. The same CCD and a diffraction grating of 600 lines mm^{-1} were used with the Coudé spectrograph to obtain the medium-resolution spectra ($R = 9000$), except for some stars where other CCDs were used (1152 × 770 pixels and 578 × 385 pixels). To confirm the spectral classification, some stars were reobserved at La Silla with the 1.52 m ESO telescope using the Boller & Chivens Cassegrain spectrograph ($R = 5000$). Reduction of the spectra collected at OPD was performed in a standard way using the IRAF package, while the ESO data were reduced with the MIDAS package. All the spectra are not flux calibrated, so each spectrum has been continuum-normalized.

The high-resolution spectra were collected with the Coudé Auxiliary Telescope using the Hamilton Echelle Spectrograph at Lick Observatory and the ESO 1.52 m telescope using the FEROS echelle spectrograph. The reduction of the Lick data was performed in a standard way described by Valenti (1994) and the FEROS reduction was automatically performed on-line by MIDAS routines. Both reduction packages include flat fielding, background subtraction, removal of cosmic rays, wavelength calibration, and barycentric correction.

Spectral types, in most cases, were determined from limited spectral range around Hα using a grid of standards (Torres 1999). The mean uncertainty in this type of determination, using stars classified in the literature as comparison, is about one spectral subtype for the B stars and two for the A and F ones. Nevertheless, since the spectral range is limited and not very adequate for spectral classification at those temperatures, we can exceptionally expect greater errors (up to five subtypes). Our proposed spectral types are in Table 1, and the corresponding effective temperatures (Kenyon & Hartmann 1995) in Table 2.

4. SPECTROSCOPIC ANALYSIS

4.1. Hα *Line Profiles*

During our 9 yr of observations, 22 stars were observed more than once. Eight of them changed their Hα line profile

TABLE 2

Photometric Observations of Herbig Ae/Be Candidates

PDS (1)	V (2)	$U-B$ (3)	$B-V$ (4)	$V-R$ (5)	$R-I$ (6)	log T_{eff} (7)
002	10.87	0.01	0.38	0.23	0.23	3.829
004	10.66	0.23	0.37	0.21	0.25	3.979
168	17.30	-	-	2.20	1.65	3.850
172	7.57	0.04	0.14	0.09	0.11	3.941
174	12.84	−0.11	0.81	0.66	0.76	4.272
176	9.84	0.17	0.17	0.10	0.11	3.979
178*	7.78	0.08	0.25	0.16	0.17	3.940
179	9.68	0.08	0.22	0.09	0.11	3.979
180	10.14	0.11	0.33	0.16	0.19	3.880
114	10.02	0.09	0.09	0.06	0.07	4.021
183	8.31	0.12	0.28	0.18	0.21	3.880
184	10.10	0.12	0.20	0.14	0.16	3.965
185S	6.49	−0.24	0.03	0.04	0.05	4.076
187	12.79	0.22	0.37	0.23	0.37	3.980
190	9.27	−0.12	0.03	0.04	0.05	4.021
191	8.88	0.05	0.13	0.05	0.07	3.965
192	9.88	0.09	0.32	0.20	0.24	3.857
193	13.85	-	1.50	1.02	1.07	4.021
194	9.80	0.12	0.16	0.09	0.15	3.914
198	13.72	1.00	1.62	1.08	1.10	3.857
016	9.01	−0.02	0.06	0.07	0.08	4.021
201	8.92	0.23	0.35	0.21	0.23	3.895
204	12.80	−0.27	0.92	0.82	0.68	4.405
018	13.40	0.69	1.48	1.05	1.12	4.114
019	13.91	0.37	1.05	0.67	0.69	4.188
020	10.64	−0.07	0.05	0.04	0.00	4.077
021	10.38	−0.37	0.30	0.26	0.25	4.188
022	10.23	0.04	0.13	0.09	0.08	3.979
207	14.01	-	1.29	0.87	1.01	4.000
124	12.44	0.18	0.53	0.29	0.34	3.979
211	13.73	0.26	0.85	0.57	0.68	3.980
126	11.82	0.32	0.53	0.30	0.36	3.895
216	14.67	0.00	1.00	0.94	0.74	4.342
023	13.52	0.30	1.39	0.95	1.01	4.400
024	13.26	0.32	0.36	0.28	0.29	3.940
130	13.40	0.36	0.66	0.44	0.52	3.979
225	6.91	−0.77	0.04	0.12	0.14	4.271
025	12.50	0.18	0.55	0.34	0.37	3.941
229*	13.13	0.12	0.57	0.39	0.50	3.979
234	15.04	-	1.19	1.10	0.89	4.500
241	12.06	−0.38	0.65	0.61	0.34	4.477
027	13.00	0.29	1.32	1.00	1.02	4.340
249	14.20	0.06	0.53	0.46	0.53	3.980
250	15.01	-	1.37	1.04	1.03	4.480
133	13.13	−0.04	0.48	0.34	0.29	4.140
255	13.02	−0.35	0.64	0.65	0.39	4.400
134	12.20	−0.11	0.41	0.28	0.27	4.146
257	15.45	-	0.90	0.66	0.73	4.000
QT2	11.97	0.21	0.64	0.40	0.39	3.821
272	9.82	0.08	0.10	0.06	0.10	3.979
277	9.96	0.05	0.41	0.25	0.25	3.829
031*	8.50	−0.11	0.00	0.01	0.00	3.979
QT3	7.23	−0.58	−0.10	−0.04	−0.06	4.207
033	12.34	0.22	0.29	0.18	0.19	3.979
034	13.99	0.02	0.76	0.55	0.62	4.270
281	8.87	−0.03	0.59	0.37	0.42	4.188
286	12.15	0.48	1.76	1.24	1.15	4.400
290	14.51	−0.07	0.69	0.48	0.55	4.000
297	12.03	0.16	0.31	0.20	0.24	3.895
303	9.26	−0.03	0.05	0.04	0.06	3.979
037	13.54	0.50	1.52	1.16	1.17	4.340
315	10.86	−0.71	0.21	0.20	0.19	4.550
322N	12.01	−0.46	0.25	0.16	0.19	4.342
324	14.45	−0.14	0.90	0.62	0.68	4.404
327	8.47	−0.71	0.13	0.11	0.12	4.405
339	7.78	0.03	0.29	0.18	0.18	3.869
340	6.75	−0.09	−0.01	0.03	0.00	4.021
057	9.24	0.15	0.18	0.11	0.13	3.979
344	13.15	−0.31	0.25	0.20	0.18	4.188
139	13.31	0.10	1.41	0.89	0.93	4.477
061	6.59	−0.03	0.21	0.17	0.18	3.979
140	13.11	0.62	1.17	0.77	0.73	3.838
353	13.21	0.11	0.82	0.76	0.68	4.188
361	12.85	−0.25	0.50	0.36	0.40	4.272
QT4	11.48	0.24	0.46	0.29	0.34	3.897
364	13.46	−0.08	0.47	0.41	0.42	4.150
371*	15.70	-	1.50	0.95	0.99	4.500
067	13.50	0.30	1.53	1.15	1.04	4.500
069*	9.80	−0.20	0.32	0.30	0.38	4.272
389	14.18	-	1.87	1.14	1.12	3.940
394	13.54	0.37	0.81	0.52	0.55	3.857
395	8.40	0.03	0.24	0.14	0.15	3.880
144*	12.79	0.31	0.49	0.30	0.33	3.980
398A	7.13	0.05	0.10	0.05	0.06	3.979
399*	8.64	−0.48	0.56	0.43	0.44	4.340
076	8.67	0.25	0.50	0.32	0.34	3.857
406	13.93	0.62	0.61	0.39	0.41	3.914
078	8.18	0.11	0.35	0.24	0.26	3.914
080	9.10	0.38	0.52	0.31	0.34	3.848
415N	12.04	0.47	0.92	0.57	0.62	3.857
431	13.42	0.21	0.57	0.40	0.43	3.979
453	12.92	0.25	0.78	0.48	0.53	3.838
095	10.98	−0.14	0.60	0.45	0.46	4.230
096	11.03	−0.31	0.30	0.27	0.34	4.190
465	12.87	−0.03	0.97	0.88	0.85	4.340
469	12.77	0.30	0.56	0.38	0.44	3.979
473	6.89	0.11	0.10	0.07	0.09	3.979
477	14.42	0.13	1.12	0.94	0.95	4.477
514	8.15	−0.02	0.28	0.19	0.20	3.979
518	12.18	1.29	2.10	1.96	1.42	4.500
520	14.69	-	1.65	1.30	1.20	3.829
530	14.04	0.37	0.57	0.42	0.50	3.910
543	12.52	0.47	2.04	1.27	1.29	4.477
545	8.84	−0.25	0.59	0.38	0.41	4.342
551	16.60	-	-	1.50	1.27	4.500
564	7.39	0.09	0.08	0.05	0.05	3.941
581	11.65	−0.29	0.67	0.62	0.54	4.410

Notes.—Photometric observations in cols. (2)–(6), and effective temperatures in col. (7). The two stars marked with an asterisk are double and the integrated magnitudes were used. A hyphen means that there is no measurement.

from single to double peak or vice versa, and three maintained the double-peaked profile while the primary and secondary peaks exchanged their positions, and 11 remained with the Hα profile stable, showing only minor changes in the intensities.

Any model that aims to explain the Hα variations needs systematic observations of the Hα line and preferentially also some data covering other wavelengths, including several emission lines, to constrain the many model parameters. There are some recent works on line-profile modeling

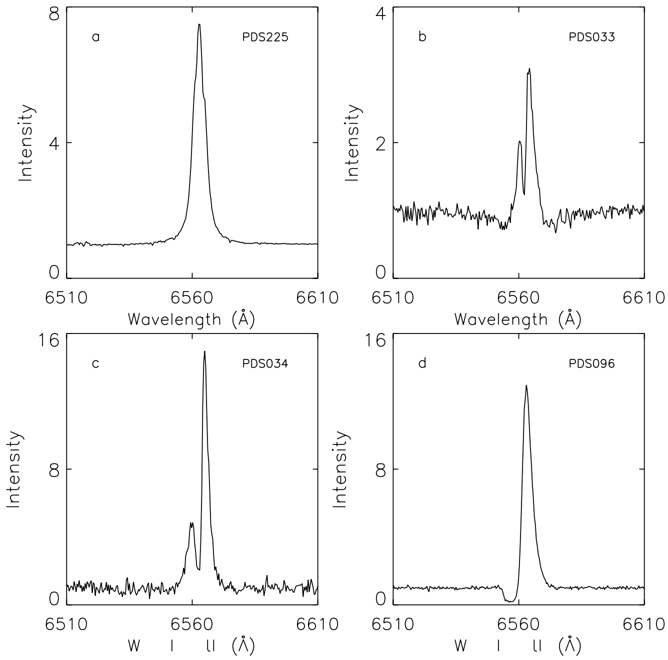

FIG. 3.—Examples of observed line profiles with the classification proposed by Reipurth et al. (1996). (*a*) Type I; (*b*) type II; (*c*) type III; and (*d*) type IV.

of HAeBe stars (e.g., Shevchenko 1999; Bouret & Catala 1998; Strafella et al. 1998; de Winter et al. 1999), which use different approaches to explain the Hα line profiles and/or their variations. They use clumpy circumstellar environments, magnetic fields, winds with velocity gradients, rotation, or combinations of two or more scenarios. A short discussion of the HAeBe models can be found in Reipurth et al. (1996).

Reipurth et al. (1996) proposed a classification system for Hα line profiles in PMS objects. In this system they are separated in four groups, exemplified in Figure 3 and as follows:

1. Type I profiles are symmetric without, or with only very shallow, absorption features.
2. Type II profiles are double-peaked, with the secondary peak having more than half the strength of the primary.
3. Type III profiles are double-peaked, with the secondary peak having less than half the strength of the primary.
4. Type IV profiles have P Cyg line characteristics.

The objects in our sample present Hα line profiles according to this system as follows:

1. type I: 29 stars (24%);
2. type II: 53 stars (43%);
3. type III: 23 stars (18.5%);
4. type IV: 18 stars (14.5%).

This distribution of line profiles agrees with what was found by Reipurth et al. (1996) with a totally different and independent sample, type II being the most common and type IV the least common line profile among HAeBe stars. This fact suggests that most of the time a HAeBe star will present type II Hα line profile.

Some authors (e.g., Vieira et al. 1999; Beskrovnaya et al. 1998) made a systematic study of the HAeBe stars HD 100546 and HD 163296 and explained the variations in their Hα profile by planetesimal bodies orbiting near the star and interaction of the wind with the circumstellar environment, respectively. PDS 034 and PDS 033 showed Hα profile variations similar to those observed in HD 100546 and HD 163296 (Figs. 4 and 5), deserving a more accurate study to confirm whether this kind of behavior can be explained by the same models.

Another interesting variation observed in double-peaked profiles is the flip over of the blue and red peaks, probably caused by the presence of a density structure (cometary bodies) in the circumstellar disk (Telting et al. 1994; de Winter et al. 1999). Two stars in our sample, PDS 018 and PDS 024 (Fig. 6), had profile variations that may be explained by this scenario. Again, it is important to notice that systematic observations are needed to confirm this hypothesis.

Because of the high variability of the Hα line profiles in a period of months, weeks, or even days, it is important to notice that the line profile is not correlated to the stellar mass or the stellar evolutionary status, the proposed classification being a snapshot of the current star properties. The objects that changed their Hα line profile from one type to another were classified using the most recent available spectrum. Since they are only eight stars, our choice does not affect significantly our statistics. Another group of seven

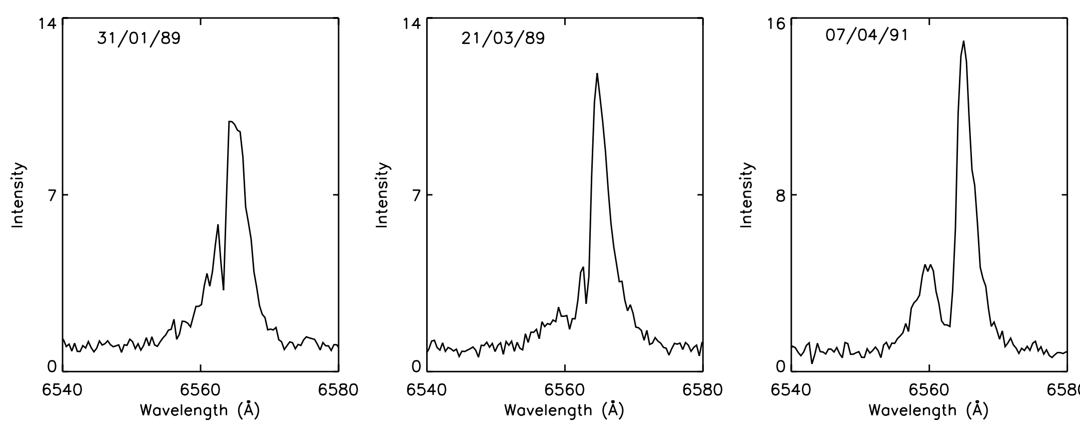

FIG. 4.—Hα line profile of PDS 034 observed in three different epochs. One can see the line profile changing from type I with humps (*left*) to type III (*right*).

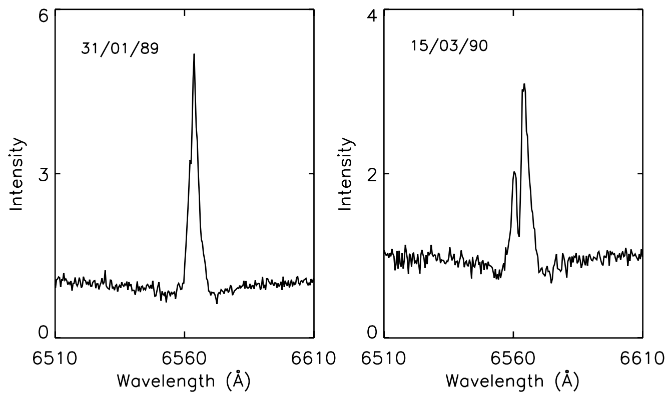

FIG. 5.—Hα line profile of PDS 033 observed in two different epochs. The line profile changed from type I (*left*) to type II (*right*).

objects has a very poor S/N, and it is impossible to assign any of the discussed types to them.

We also tried to associate the line-profile distribution with the index β (defined in § 2), but no correlation was found.

In a similar work with a smaller sample (57 objects) Finkenzeller & Mundt (1984) found that stars with type IV line profiles were clustered among B8 to A0 spectral types. We do not verify in our sample such a correlation between spectral type and Hα line profile. The 18 stars presenting type IV profile are evenly distributed among all spectral types (see Table 1).

We also tried to find some correlation between the Hα line-profile type and the projected rotational velocity ($v \sin i$). Only 29 of our stars presented visible absorption lines with a reasonable S/N that could be used to determine $v \sin i$. We gathered atomic line data from the Vienna Atomic Line Database (VALD, Piskunov et al. 1995) and used the SME line synthesis code (Valenti & Piskunov 1996)

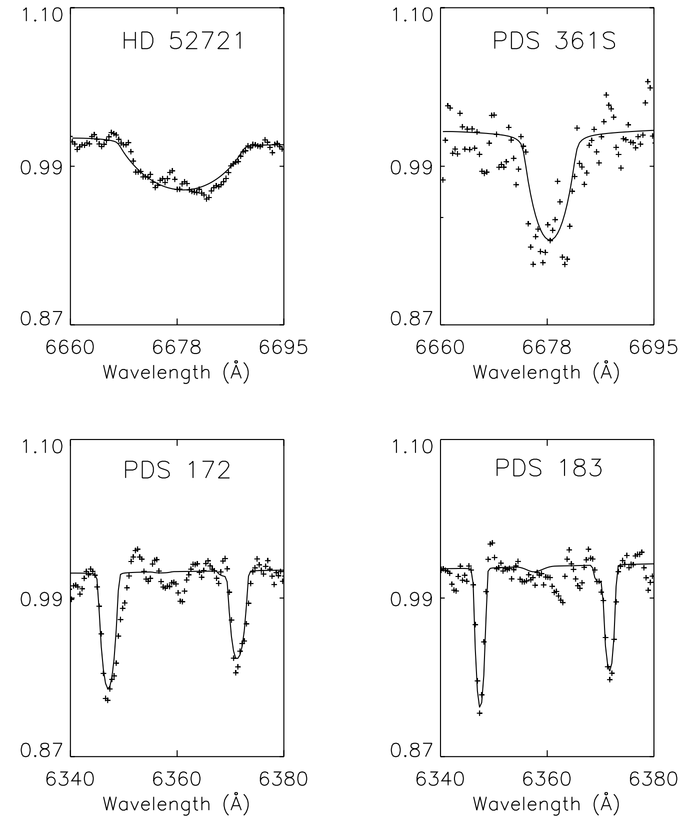

FIG. 7.—Sample of fitted (*solid lines*) and observed (*plus signs*) spectra for four HAeBe objects with different values of $v \sin i$.

to fit the absorption lines and determine the rotational velocities.

We used three absorption lines observed in the following wavelengths: 6347, 6371, and 6677 Å. The initial parameters used in the SME code were effective temperature, log g, and microturbulence and macroturbulence velocities (taken from Gray (1992) according to the stellar spectral type); these estimates led to a good fitting for $v \sin i$ (Fig. 7). The measured $v \sin i$ and the corresponding Hα line-profile types and spectral types of the 29 stars are presented in Table 3.

We did not find any correlation between spectral type and $v \sin i$. As one can see from Table 3, there is also no correlation between Hα profile type and $v \sin i$ for types I, II, and III. However, all stars presenting Hα type IV line profiles have rotational velocities clustered below $\sim$100 km s^{-1}. This fact is expected, since stars with P Cyg line profiles are expected to have strong winds and consequently strong mass loss, rapidly loosing angular momentum and being slow rotators.

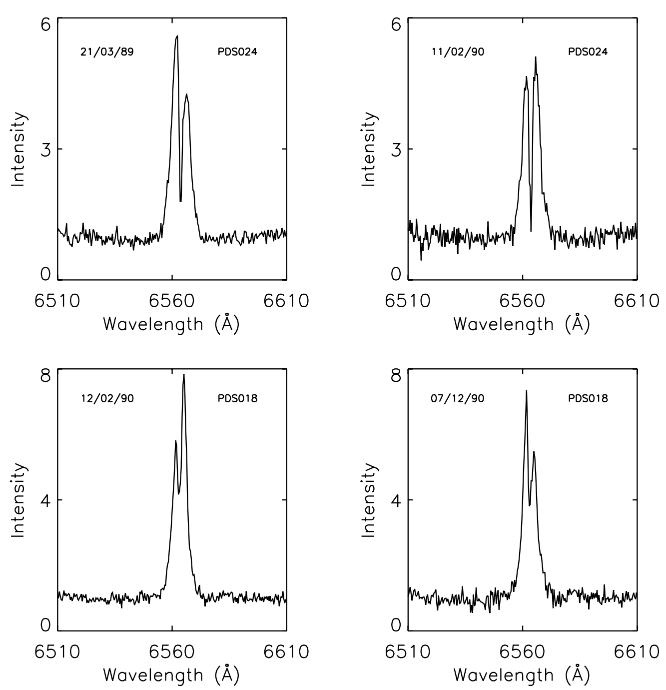

FIG. 6.—Hα line profiles of PDS 024 and PDS 018 observed in two different epochs. One can see the flip over of the red and blue peaks.

4.2. [O I] (6300 *and* 6364 Å) *and* [S II] (6716/6731 Å) *Forbidden Lines*

Using the low-, medium-, and high-resolution spectra obtained for all the stars, [O I] and/or [S II] lines were detected in 59 out of 128 objects (three stars have spectra beginning at 6500 Å, and we consequently cannot say anything about the presence of [O I]). This amount corresponds to 46% of our sample, and it can be regarded as a lower limit since we do not have high-resolution spectra of all the stars and could therefore be missing some low-intensity

TABLE 3

Rotational Velocities for Herbig Ae/Be Candidates

Object	$v \sin i$ (km s^{-1})	Type	Sp. Type
PDS 225	225	I	B3
PDS 514	58	I	A0 V
PDS 002	175	I	B0 V
PDS 564	88	I	A3 V
PDS 395	52	I	A8 V
HD 52721	456	I	B2 Vn
PDS 174	144	II	B3
PDS 180	125	II	A8 V
PDS 327	132	II	B1
PDS 361	190	II	B3
PDS 398A	281	II	A0 V
PDS 545	238	II	B2
PDS 076	97	II	F0 V
PDS 080	120	II	F1 III
HBC 282	142	II	B+sh
HD 95881	74	II	A0
HBC 552	128	II	F+sh
HD 76534	116	II	B2
PDS 069N	158	III	B3
PDS 339	100	III	A9 V
HBC 551	245	III	B5
HD 53367	55	III	B4
PDS 183	59	IV	A8 V
PDS 315	44	IV	O8
PDS 172	90	IV	A3 V
PDS 201	119	IV	A7 V
HD 98922	52	IV	B9
HBC 078	85	IV	A5 V
HD 150193	103	IV	A0 V

forbidden lines in the low- and medium-resolution observations. In some cases, however, forbidden lines detected in low- and medium-resolution spectra were not present in the high-resolution observations (taken at a different epoch), suggesting that those lines also present variable intensities.

The distribution of the detected forbidden lines among different spectral types and Hα line-profile types can be seen in Table 4. We have an almost equal number of A (40%) and B (45%) stars in our sample; therefore, the results in Table 4 point to a significantly higher occurrence of forbidden lines among B stars. The forbidden line distribution among different Hα profile types is nearly identical to the Hα profile distribution in our sample (see § 4.1), indicating that forbidden lines are evenly distributed among each Hα line-profile type.

In a previous work Böhm & Catala (1994) detected [O I] in stars with Hα line profiles of types II, III and IV and did not detect it in stars with type I profiles. Since types II, III, and IV are characteristic of stars with stellar winds and [O I] is expected to originate in jet/outflow regions associated with mass-loss processes, they suggested that objects with type I profiles do not present stellar winds or have very low mass-loss rates. As can be seen in Table 4, 29% of the [O I] lines detected by us belong to type I stars, leading us to believe that the Böhm & Catala (1994) sample is strongly affected by selection effects in this aspect.

The distribution in our sample of [O I] and [S II] forbidden lines supports the results of Corcoran & Ray (1997, 1998), who also found that the forbidden lines are concentrated among B type stars and are observed among type I Hα line-profile stars. Corcoran & Ray (1997, 1998), however, found that forbidden lines were more common among type II line profiles, while our results point to an equal distribution among all profile types. Selection effects may explain their results, since the majority of their stars belong to group II in the work of Hillenbrand et al. (1992), which generally presents Hα line profiles of types II and III.

TABLE 4

Distribution of the Forbidden Lines among Different Spectral Types and Hα Line-Profile Types

Type	Distribution (%)
Spectral Type	
B	54
A	30
F	8
O	8
Hα Profile	
I	29
II	41
III	18
IV	12

5. DISCUSSION AND ANALYSIS

5.1. *Circumstellar Environment*

The Balmer line profiles and the presence of forbidden lines are strongly connected with the circumstellar environment. To check this correlation, we use SEDs calculated for 62 HAeBe stars in our sample by M. Sartori & J. Gregorio-Hetem (private communication), using the disk model of Gregorio-Hetem & Hetem (2002). In this model the star is surrounded by an extended and flat disk and a thin dust

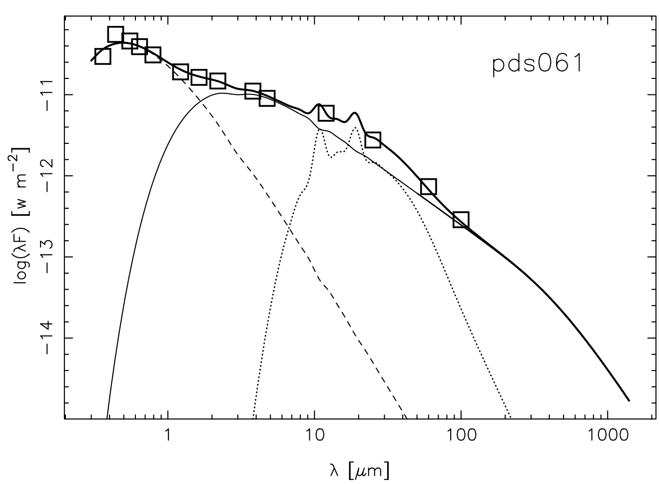

Fig. 8.—Example of SED fitting using the model of Gregorio-Hetem & Hetem (2002). The solid thick line is the resulting total emission, and different lines are used to show contributions from the star (*dashed line*), the disk (*solid line*), and the envelope (*dotted line*). The observed data are represented by open squares.

shell envelope. The disk is assumed to be passive, optically thick, and geometrically thin. The inner radius of the disk is constrained by the adopted grain destruction temperature (1500 K), and the outer disk radius defines the inner radius of the envelope. The total radiation emitted is the sum of the contributions of the star, the disk, and the envelope. In this preliminary analysis the disk and envelope contributions were not disentangled. We will only discuss stellar and circumstellar (disk+envelope) contributions to the SED.

The stellar contribution is calculated assuming a blackbody emission attenuated by the opacity of the envelope (see § 3 of Gregorio-Hetem & Hetem 2002). The star temperature that defines the blackbody is obtained from the calibration between spectral type and effective temperature proposed by de Jager & Nieuwenhuijzen (1987) for main-sequence stars. The optical depth used in the calculation of the attenuation is initially estimated by the observed color excess $E(B-V)$ and then iterated during the model fit.

The observational data used to fit the model are composed of *UBVRI* photometry, *IRAS* far-infrared fluxes, and, whenever available, *JHK* 2MASS photometry. The SED calculations will be discussed in detail in a companion paper. An example of an SED fit is presented in Figure 8.

Figure 9 shows histogram plots of the circumstellar contribution to the SED versus the total number of stars (*a*), the stars presenting forbidden lines (*b*), and the Hα line profile types (*c*, *d*, *e*, and *f*).

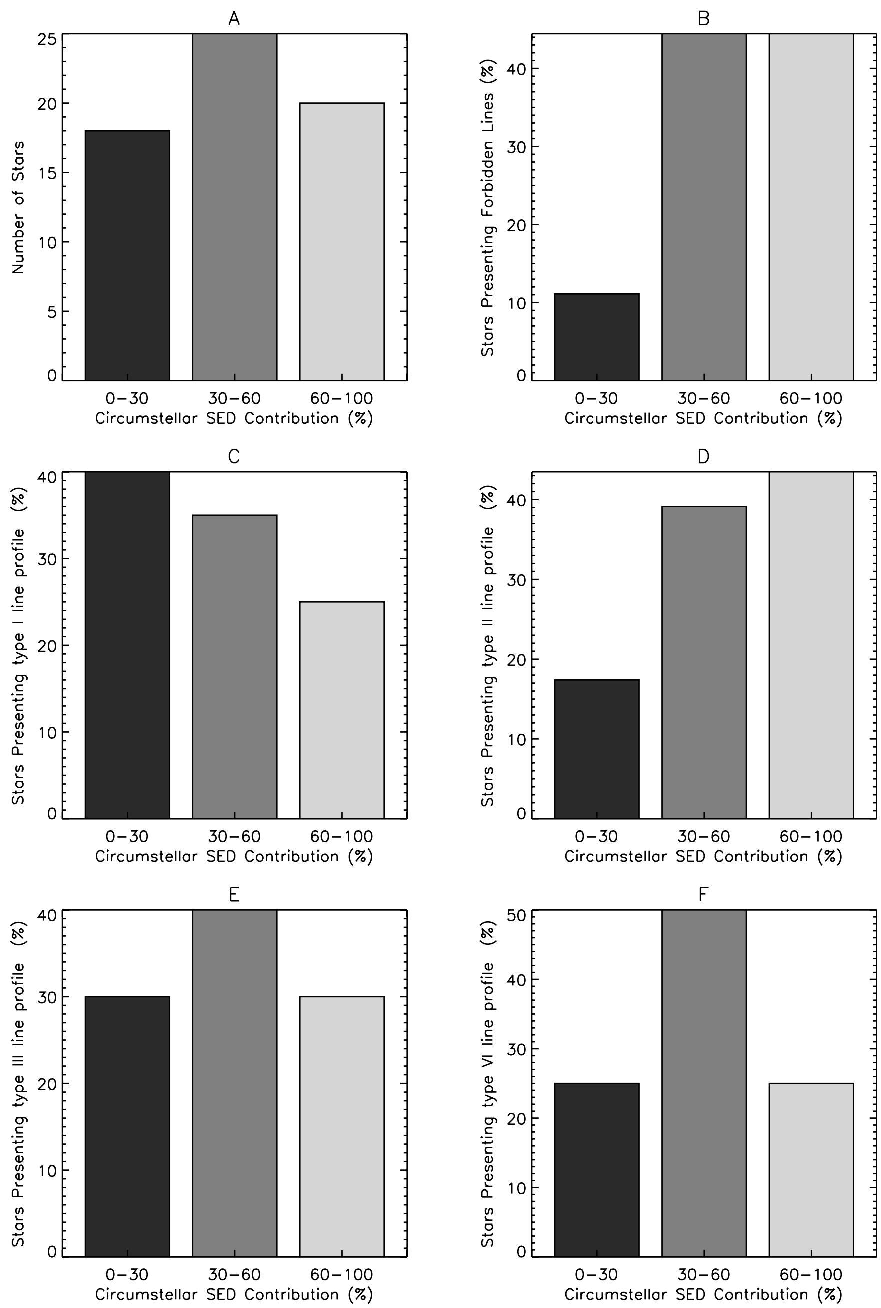

FIG. 9.—Distribution of HAeBe stars according to the circumstellar contribution to the SED. (*a*) All the HAeBe stars in our sample; (*b*) stars presenting forbidden lines; and (*c*)–(*f*) stars according to their Hα line-profile types.

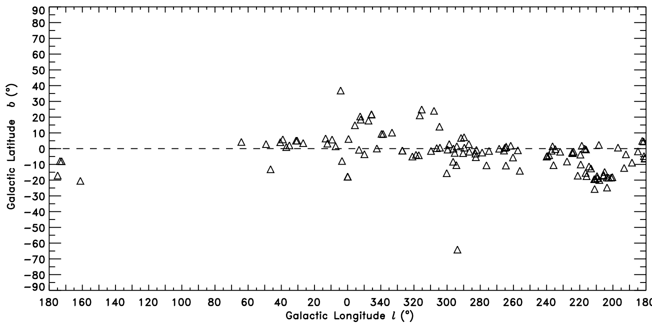

FIG. 10.—Distribution of the PDS HAeBe stars in Galactic coordinates.

We can see from Figure 9 that forbidden lines are concentrated in objects that have significant circumstellar contribution. We also notice that Hα line-profile types present the following distribution: type I line profiles are concentrated around objects with less significant circumstellar contribution, type II in the more significant circumstellar ones, and types III and IV represent intermediate situations with a histogram peaking at objects that present 30%–60% of circumstellar contribution to the SED.

5.2. *Galactic Distribution*

To improve the proposed classification of the HAeBe candidates found in the PDS, minimum distances were calculated assuming that the stars are on the main sequence. It is important to keep in mind that these are only indicative values, since HAeBe stars may have strong photometric variations and our estimates of the reddening are independent of the galactic environment as the factor R is obtained in the same way.

We used these minima distances to investigate the possible relationship between the candidates and the main star-forming regions (SFRs). Figure 10 shows a plot of the Galactic distribution of the HAeBe candidates. As one can see, the stars are concentrated around the Galactic plane, mostly between $-25° \leq b \leq 25°$.

To further investigate the connection between stars and star-forming regions, we plotted in Figure 11 the HAeBe stars over the opacity levels of the photographic Dark Clouds Catalogue compiled by Feitzinger & Stuwe (1984). Around $l \approx 270°$ there is a well-known tunnel of low reddening near the Galactic plane, which allows us to find HAeBe candidates even at great distances. Figure 12 shows the HAeBe stars in the Orion region superposed on the contours of the larger molecular clouds found by the Columbia millimeter-wave telescope in the third Galactic quadrant (Maddalena et al. 1986).

Combining the distance estimates of the Herbig candidates with the knowledge of the interstellar medium distribution, we have found that 84 candidates seem to be associated with some of the more conspicuous SFRs, being in the right direction and at a compatible distance. For 24 stars the proposed association is not clear enough within the given uncertainties. Two candidates do not have photometric data and no other indicator of their distance could be found. In this case only a positional coincidence with the SFR could be given. Another two candidates were not considered in this analysis since they have been recently recognized as a protoplanetary nebula: PDS 465 (García-Hernández et al. 2002) and PDS 581 (Castro-Carrizo et al. 2002).

The results are summarized in Table 5. The first column contains the star identification in the PDS catalog, except where otherwise noted. The following columns contain the Galactic coordinates l and b in degrees, the photometric and *Hipparcos* distances of the star in parsecs, the distance and name of the proposed star-forming region associated to the HAeBe candidate, as well as its reference in the literature. The last column contains general comments, such as other HAeBe designations or suggestions of associated star-forming regions. The other 19 stars used to complement the data are also listed at the end of the table.

When available, *Hipparcos* distances were preferred. In some cases we were able to find kinematic distances ($d_{\rm kin}$) to the SFR. It should be noted that the photometric distances were calculated assuming that the stars are in the main sequence. Therefore, to be certain of the association of HAeBe candidates and SFR, we need to improve the distance determination of the stars, especially of the more distant ones, as well as the distance of the less well-studied SFRs. Given such limitations, caution should be exercised in using the proposed associations.

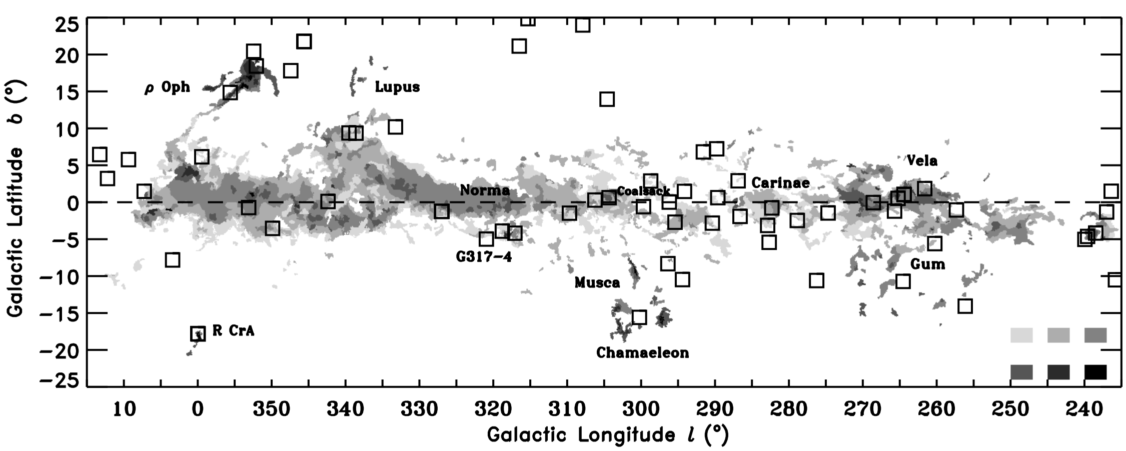

FIG. 11.—Location of the PDS HAeBe stars (*squares*) within the studied area. The clouds' contours are the lowest opacity level of the photographic catalog by Feitzinger & Stuwe (1984).

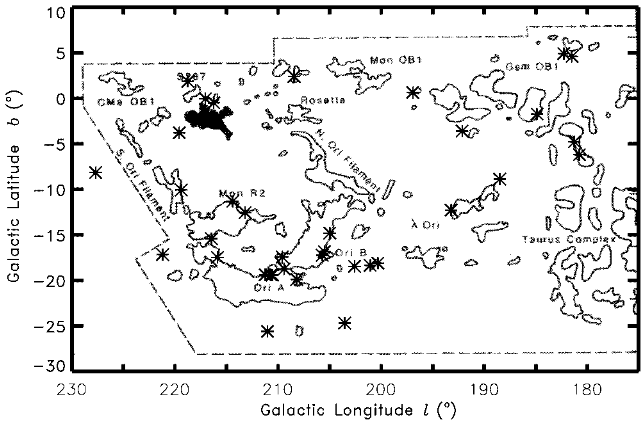

FIG. 12.—PDS HAeBe stars in the Orion region superposed on the contours of the larger molecular clouds found by the Columbia millimeter-wave telescope in the third Galactic quadrant (Maddalena et al. 1986).

5.3. *Evolutionary Status*

As a further means of checking the properties of the HAeBe candidates, as well as their present evolutionary status, the derived luminosities (calculated according to Balona 1994) and effective temperatures of stars in Table 2 were plotted together with a set of PMS evolutionary tracks on an HR diagram, as shown in Figure 13. The luminosities were calculated using the distances and errors from *Hipparcos*, when available, or to the associated SFR and their uncertainties, as explained in the previous section.

The evolutionary tracks were computed using the ATON 2.0 stellar evolution code (Mazzitelli 1989; Mazzitelli et al. 1995; Ventura et al. 1998). The input physics for all models were the same, namely, opacities taken from the OPAL (Iglesias & Rogers 1993) opacity tables, supplemented by those at low and intermediate temperatures of Alexander & Ferguson (1994); the convection model was the standard mixing length theory, with α (ratio of the mixing length to the pressure scale height) set to 1.5, and the chemical composition was set to the solar one ($Y = 0.271$, $Z = 0.0175$), which is typical of Population I stars.

As one can see, most HAeBe candidates not only are located within the usual mass range (2–10 $M_{\odot}$) for HAeBe stars but are also near the ZAMS. The group of stars with masses between 1.5 and 2 $M_{\odot}$ is expected in our sample, since the selection criteria of HAeBe stars adopted by the PDS program included stars earlier than F5.

Considering the error bars, a set of 14 stars (Table 6) has luminosities and temperatures that put them out of the expected position for an HAeBe object, all of them deserving more accurate study. The stars above the considered mass range (Table 6) include two that are suspected to be protoplanetary nebulae: PDS 067 (Miroshnichenko et al. 1999) and PDS 234 (Garcia-Lario et al. 1993, 1997). Regarding the stars below the ZAMS, three of them are classified as HAeBe objects: PDS 176 (van den Ancker et al. 1998; Piétu et al. 2003), PDS 004 (Miroshnichenko et al. 1999), and PDS 193 (Thé et al. 1994).

5.4. *Evolved HAeBe Objects*

During the evolution of HAeBe stars the circumstellar disk or envelope is cleared by planetesimal or cometesimal bodies and stellar winds. In this evolutionary stage the disk

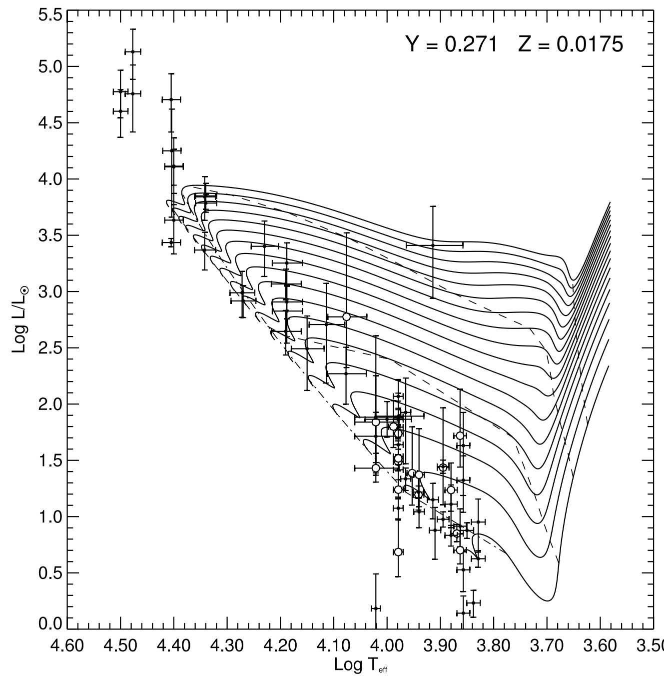

FIG. 13.—Evolutionary tracks from 1.5 up to 10 $M_{\odot}$ (*solid lines*) and the isochrones corresponding to 10^3, 10^4, 10^5, and 10^6 (*dashed lines*) and 10^7 (*dash-dotted line*), respectively. The stars with distances taken from SFR are shown as dots. The big open dots are stars with *Hipparcos* distances.

(envelope) contribution to the Hα emission is very weak and the Hα line is almost totally formed at the stellar chromosphere. Sometimes the remote and cool shell is responsible for a central absorption.

The following objects have Hα line profiles that might be explained by this evolutionary scenario (Fig. 14): PDS 031S, 080, 179, 201A, 281, 290, and 303. For three of them (PDS 031S, 080, and 201) the SED was calculated and the circumstellar contribution is very low: 12.3% for PDS 031S, 31.4% for PDS 080, and 27% for PDS 201.

6. CONCLUSIONS

Although HAeBe objects present a great variety of Hα line profiles, our study shows that the type II line profile seems to be the most common. This is the same result as that of Reipurth et al. (1996), with a different sample, suggesting that most of the time a HAeBe star will present a type II Hα line profile. A correlation between the Hα line profile and $v \sin i$ was only found for stars that have a type IV line profile, which is expected because the stellar wind causes the loss of angular momentum, and these stars will become slow rotators.

In our sample [O I] and [S II] forbidden lines and Hα type II line profiles are concentrated in objects that have a strong circumstellar contribution to the SED. The forbidden lines also tend to occur more frequently among B than A stars, supporting the results of Corcoran & Ray (1997, 1998).

The distribution of forbidden lines among different Hα line profiles is the same as the distribution of objects among Hα profile types. This fact shows that there is no correlation between the presence of forbidden lines and the Hα line-profile type, contrary to what was found by Corcoran & Ray (1997, 1998) and Böhm & Catala (1994). It is important

TABLE 5

PDS Stars and Their Proposed Star-Forming Regions Association

Name	l	b	d_{phot}	d_{Hip}	d_{SFR}	SFR	Ref.	Comments
Taurus-Auriga								
004	161.19	−20.46	580	...	250–300	Per OB2	4	V1185 Tau
168	174.87	−17.06	130	...	130–150	LDN 1536	1	...
172	173.47	−7.90	150	131^{156}_{115}	140–160	Tau	2	HD 31648
178N	180.76	−6.19	220	150^{236}_{110}	140–160	LDN 1554	3	...
178S	180.76	−6.19	220	150^{236}_{110}	140–160	LDN 1554	3	...
183	181.26	−4.77	140	204^{268}_{165}	140–160	Tau	2	...
Gemini								
020E	192.14	−3.60	1200	...	1000–1500	Gem OB1	5, 6	...
204	184.88	−1.73	2600	...	1100	WB 711	1993	BFS 50
Orion								
016	209.59	−17.43	480	422^{935}_{272}	460–650	Ori OB1	8	...
018	215.88	−17.48	380	...	300–700	Ori A	7	...
023	219.39	−10.06	1700	...	670–1130	Southern Ori	10	Mon R2 ($d = 830$ pc)
114	202.58	−18.46	730	...	460–650	Ori OB1	8	LDN 1614
176	211.03	−25.61	540	164^{224}_{129}	300–460	Ori	7	V1366 Ori
179	200.32	−18.11	470	952^{-}_{330}	460–650	Ori OB1	8	...
180	201.07	−18.34	300	645^{-}_{280}	300–460	Ori	7	...
184	193.21	−12.28	510	...	360–440	λ Ori	9	V1409 Ori
185S	188.50	−8.88	180	342^{742}_{223}	360–440	λ Ori	9	HR 1847
190	205.71	−17.25	550	...	300–700	Ori A	7	...
191	210.56	−19.41	320	...	300–700	Ori A	7	vdB 46
192	205.50	−16.84	270	...	360–640	Ori B	7	V1247 Ori, vdB50
193	210.72	−19.38	600	...	300–700	Ori A	7	...
194	209.40	−18.73	230	...	300–700	Ori A	7	...
198	211.25	−19.39	190	...	300–700	Ori A	7	V599 Ori
201	204.98	−14.81	170	285^{521}_{196}	460–650	Ori B	7	V351 Ori
Canis Major								
024	227.69	−8.15	1800	...	2000	CMa	10	...
025	235.81	−10.50	790	...	660–730	Collinder 121	10, 48	...
027	231.81	−1.96	1100	...	1200–1300	CMa	10, 14	...
133	239.58	−4.63	2500	...	2460	LDN 1664	1, 12	...
134	237.00	−1.32	1800	...	2090	SS 127	12	...
229N	216.23	−0.49	1600	...	1300–1600	Mon	14	...
234	217.05	−0.05	4200	...	3000–4600	Sh 2-287	46	Iron Clad neb.
241	218.75	1.86	3900	...	5300–8300	Sh 2-288	46	Ced 92
249	239.94	−5.03	2300	...	2460	LDN 1664	1, 12	...
255	234.77	−0.27	4500	...	3000–5400	Sh 2-309	12, 46	...
257	236.38	1.49	3000	...	4300	G236.4+1.49	12	...
Monoceros								
021	216.46	−15.42	1100	...	1000–1200	LDN 1653-1656	1, 10	V791 Mon
022	221.20	−17.16	690	...	780–880	NGC 2149	11	AE Lep
124	213.19	−12.56	1000	...	780–880	LDN 1646	13	...
126	214.40	−11.31	500	...	780–880	Mon R2	14	...
130	219.59	−3.79	1200	...	1000–2000	BFS 63	10, 46	CMa R1 ($d = 1315$ pc)
Vela and the Gum Nebula								
031S	257.63	0.25	670	288^{490}_{204}	200–240	Gum Nebula	17	...
033	261.62	1.84	1400	...	850–1150	RCW 32	46	...
034	265.70	−1.20	2900	...	1800–2190	Vela OB1	8	...
272	260.26	−5.60	600	...	500–900	Vela OB2	16, 48	...
277	257.33	−1.05	210	...	200–240	Gum Nebula	17	...
281	265.23	0.52	340	...	450–600	Vela	11, 18	...
286	268.58	−0.05	560	...	450–600	Vela	11, 18	...
290	274.70	−1.46	1800	...	1800–2190	Vela OB1	8	...
297	278.86	−2.47	770	...	700–800	DC 278.2−2.1	15, 16	...

TABLE 5—*Continued*

Name	l	b	d_{phot}	d_{Hip}	d_{SFR}	SFR	Ref.	Comments
				Carina				
037	282.31	−0.77	720	...	800	DC 282.4+0.5	17	SA 192
303	282.88	−3.14	435	...	800	DC 282.8−3.2	17	SA 192
322N	286.87	2.90	3800	...	2200–2800	Car OB1	8, 28	DC 287.7+2.9
324	290.36	−2.83	5500	...	3200–8800	G35	46	...
327	289.62	0.62	1200	...	1650–2750	Car OB2	8, 46	G37 ($d = 3200 \pm 500$)
339	291.58	6.81	110	111_{102}^{121}	120–150	Carina	19	SA 193
				Centaurus and Crux				
057	294.13	1.47	410	...	500–700	DC 295.0+1.3	21	close to Sh 2-131
067	309.7	−1.48	1700	...	1500–2300	Cen OB1	8, 46	RCW 80 ($d = 3800 \pm 700$)
139	296.19	0.02	2200	...	1750–3250	Cru OB1	8, 46	RCW 62 ($d = 2100 \pm 300$)
140	298.70	2.87	290	...	150–200	Coalsack	21	...
353	299.68	−0.60	1200	...	900–1400	Coalsack	20	SS 73
361	304.33	0.62	2700	...	1700–2400	Cen OB1	8	...
364	306.25	0.29	2600	...	1500–2700	RCW 75	46	...
				Chamaeleon-Musca				
061	300.23	−15.59	115	116_{109}^{124}	140–200	Cha	23	DX Cha
340	296.37	−8.32	190	103_{97}^{110}	100–120	DC 296.2−7.9	22	HD 100546
				Norma				
399A	326.98	−1.24	874	...	600–700	Norma	24	...
399B	326.98	−1.24	874	...	600–700	Norma	24	...
389	318.78	−3.91	240	...	150–200	G317-4	17	Circinus
394	320.94	−4.99	670	...	400–600	Circinus	25	Sandqvist 165
406	338.59	9.35	1200	...	1000–1400	Norma	24	...
431	342.37	0.10	1300	...	1000–1400	Norma/Ara	24	...
				Lupus and Ophiuchus				
076	349.91	23.50	118	...	110–160	Sco R1	27	...
078	347.41	17.81	119	253_{183}^{405}	110–160	ρ Oph	17, 26	...
080	352.43	20.44	139	131_{114}^{154}	110–160	ρ Oph/Sco OB2	17, 8	...
095	353.11	−0.72	950	...	1100–1700	RCW 131	28	...
096	349.87	−3.54	1300	...	850–1150	DC 349.8−3.5	29, 30	vdB 91
395	333.24	10.19	160	...	130–160	Lupus	17	...
398A	4.19	36.91	170	99_{91}^{108}	110–160	ρ Oph	17, 26	...
415N	352.07	18.44	280	...	110–160	ρ Oph/Sco OB2	17, 8	LDN 1687
473	7.24	1.48	160	121_{109}^{139}	110–160	ρ Oph	17, 26	HD 163296
				Serpens, Aquila, and Scutum				
518	26.81	3.52	230	...	220	Scutum	11, 7	Aql Rift ($d = 200$)
520	31.14	5.06	180	...	200–350	Serpens	31	...
530	39.09	5.87	1000	...	600–1000	W50	32, 49	...
545	40.62	4.09	560	...	500–700	LDN 637	1	...
564	49.21	2.88	197	244_{200}^{313}	200–300	Aquila	33	...
				Stars from PDS without Clear Association to Star-Forming Regions				
002	293.76	−64.10	340	...	...	...	...	Isolated?
019	219.84	−18.12	1700	...	850–1150	Southern Ori	27	...
344	295.41	−2.70	4100	...	1300–2500	DC 296.1−2.5	8, 46	Cru OB1
069N	316.49	21.14	1200	...	100	G316.4+21.2	33	MBM 112
144N	345.61	21.77	2000	...	...	Magnani 124	36	...
144S	345.61	21.77	1030	...	...	Magnani 124	36	...
174	203.54	−24.69	1700	...	460	G203.4-24.7	33	LDN 1615/1616
187	208.19	−19.90	1600	...	300–700	Ori A	7, 46	UY Ori
207	181.48	4.60	600	...	3000–4400	LDN 1557	34, 6	...
211	182.28	4.92	1100	...	3000–4400	LDN 1557	34, 6	...
216	196.93	0.64	2700	...	850–1150	Mon OB1	7	$d_{kin} = 4700$ pc
225	208.45	2.40	360	...	930–1600	Rosette	35	$d_{kin} = 930$ pc
250	238.48	−4.17	4100	...	2460	LDN 1664	1, 12	...
315	286.61	−1.92	6500	...	2000–3000	Car OB1	8	...
371N	315.31	24.86	6000	...	...	...	...	...

TABLE 5—*Continued*

Name	l	b	d_{phot}	d_{Hip}	d_{SFR}	SFR	Ref.	Comments
Stars from PDS without Clear Association to Star-Forming Regions								
453	359.45	6.15	490	...	...	LDN 1767/1773	34	...
469	13.26	6.46	1100	...	...	LDN 330	37	...
477	12.21	3.21	2900	...	900–1500	Sgr R1	8	...
514	3.40	−7.82	130	...	...	...	...	Isolated
543	35.13	2.08	414	...	$\geq$1000	LDN 616	50	...
551	37.01	0.98	3500	...	2000	CO 38+2	49	LDN 628
QT4	307.89	24.00	457	...	...	...	...	V958 Cen
QT2	264.54	−10.72	309	...	...	DC 264.5−11.3	15	Gum Nebula
QT3	276.24	−10.60	492	...	...	DC 276.2−10.6	15	...
Stars without Distance but with Remarkable Positional Coincidence								
QT1	203.65	−18.27	...	...	360–640	Ori B	7	...
141	303.04	−14.24	...	...	140–200	DC 303−14	38	DK Cha
Stars from Other Haebe Catalogs Used To Complement the Data								
HBC 078	172.50	−8.00	...	144_{126}^{167}	140–160	Tau-Aur	2	AB Aur
HD53367	223.70	−1.91	...	250_{185}^{370}	500	vdB 86	29	V750 Mon
HD 52721	224.15	−2.87	...	910_{357}^{-}	670–1130	Southern Ori	10	...
HBC 548	224.37	−2.73	...	...	810–1150	CMa OB1	47	HT CMa
HBC 551	224.53	−2.43	...	...	810–1150	CMa OB1	47	HU CMa
HBC 552	256.14	−14.07	...	500_{228}^{-}	450	Gum Nebula	18	NX Pup
HD 76534N	264.41	1.05	...	410_{268}^{884}	450–600	Vela	40	OU Vel
HD 76534S	264.41	1.05	...	410_{268}^{884}	450–600	Vela	40	OU Vel
HD 85567	282.67	−5.43	...	1000_{591}^{3225}	800–2500	Carina	41	...
HD 98922	289.77	7.23	...	1040_{632}^{2900}	1000–2000	Centaurus	42	...
HD 95881	294.40	−10.47	...	...	...	DC 295.3−13	43	Globule 121
Hen 3-847	304.60	13.95	...	...	...	...	...	V1028 Cen
HBC 596	317.08	−4.19	...	...	150–200	G317-4	17	Circinus
HBC 619	339.53	9.38	...	210_{176}^{253}	130–160	Lupus	44	V856 Sco
HD 150193	355.60	14.85	...	150_{119}^{200}	100–140	Ophiuchus	26	...
HBC 288	359.94	−17.84	...	8_{5}^{18}	130–170	DC 359.9−17.9	45	R CrA
HBC 287	359.99	−17.78	130	...	130–170	DC 359.9−17.9	45	TY CrA
HBC 282	30.46	5.11	...	...	200–300	Aql Rift	7, 11	VV Ser
HD 190073	46.47	−13.09	...	5000_{750}^{-}	...	...	...	V1295 Aql

References.—Reference code: (1) Hilton & Lahulla 1995; (2) Cohen & Kuhi 1979; (3) Ungerechts & Thaddeus 1987; (4) de Zeeuw et al. 1999; (5) Haug 1970; (6) Carpenter et al. 1995; (7) Dame et al. 1987; (8) Dambis et al. 2001, (9) Murdin & Penston 1977; (10) Maddalena et al. 1986; (11) Feitzinger & Stuwe 1986; (12) Wouterloot & Brand 1989; (13) Herbst & Racine 1976; (14) Maddalena & Thaddeus 1985; (15) Hartley et al. 1986; (16) Lizeau et al. 1992; (17) Franco 1990; (18) Pettersson 1991; (19) Knude 1984; (20) Franco 1989; (21) Corradi et al. 1997; (22) Vieira et al. 1999; (23) Whittet et al. 1997; (24) Haug & Bredow 1977; (25) Haug et al. 1966; (26) Knude & Høg 1998; (27) Racine 1968; (28) Higdon & Lingenfelter 1996; (29) Eggen 1978; (30) Persi et al. 1991; (31) Eiroa 1991; (32) Dame & Thaddeus 1985; (33) Yonekura et al. 1999; (34) Lynds 1962; (35) Turner 1976; (36) Magnani et al. 1985; (37) Parker 1991; (38) Gregorio-Hetem et al. 1988; (39) Keto & Myers 1986; (40) Duncan et al. 1996; (41) Feinstein 1995; (42) Courtès et al. 1970; (43) Feitzinger & Stuwe 1984; (44) Tachihara et al. 1996; (45) Marraco & Rydgren 1981; (46) Avedisova 2000; (47) Herbig 1991; (48) Kaltcheva 2000; (49) Andersson 1991; (50) Myers 1975.

TABLE 6

Stars out of the Expected Position in the HR Diagram

PDS	Name
PDS 204	MWC 778
PDS 234	GSC 4805−1306
PDS 241	GSC 4823−0146
PDS 255	SS73 6
PDS 286	Hen 3-248
PDS 324	IRAS 10554−6237
PDS 327	HD 96042
PDS 139	IRAS 11507−6148
PDS 067	Hen 3-938
PDS 176	HD 34282
PDS 193	GSC 4779−0040
PDS 140	GSC 8645−1401
PDS 415N	CD −23 12840
PDS 004	GSC 1811−0767

to note that the completeness of our sample gives support to our results.

When plotted in the HR Diagram, 14 stars lie out of the expected position for HAeBe stars. Three of them were already classified as HAeBe stars and two as protoplanetary nebulae. The remaining nine objects need more study, mainly in distance determination.

An investigation of the possible relationship of the HAeBe candidates found in the PDS with the main SFR shows that 84 candidates seem to be associated with one of the more conspicuous SFRs, being in the right direction and at compatible distances. Twenty-four stars need a more accurate study in order to assign any association to them.

Still considering the Hα line profile, eight objects presented a line profile (weak emission inside the absorption well) that can be explained by an evolutionary scenario where the shell is almost absent (evolved HAeBe stars). Since HAeBe stars show great variability in the Hα line

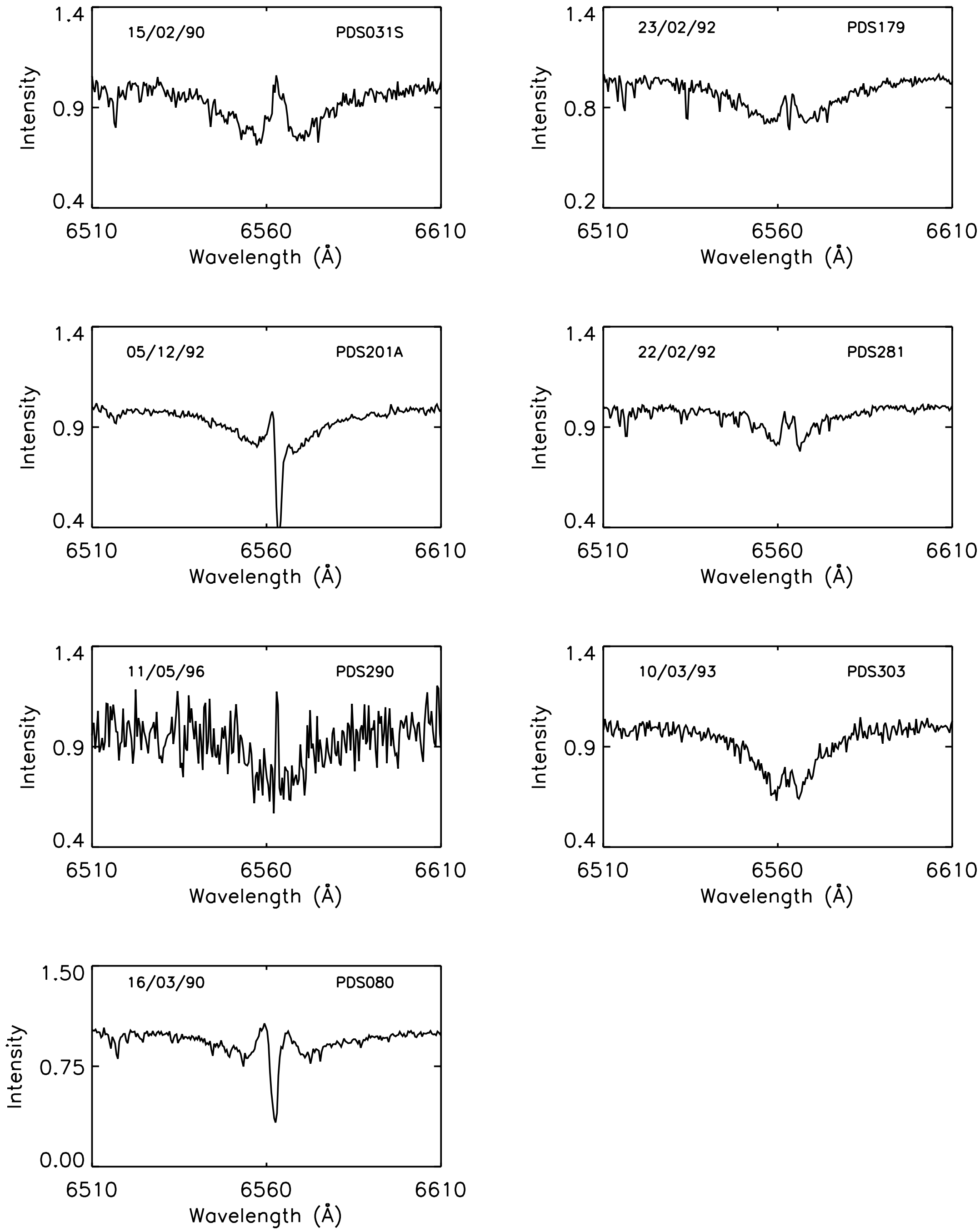

FIG. 14.—Hα line profiles of the presumably evolved HAeBe objects

profile, it is important to follow the behavior of these stars in order to confirm this classification.

The authors wish to thank M. Sartori and J. Gregorio-Hetem for the SED calculation. S. L. A. V., W. J. B. C., and L. T. S. M. acknowledge CNPq (grant 471537/2001-02) and FAPEMIG for partial financial support for doing this work. S. H. P. A. acknowledges support from FAPESP (grant 00/06244-9), and CAPES (PRODOC program). M. M. G. acknowledges support from CAPES. C. A. O. T. acknowledges support from CNPq (grant 200356/02-0). This research has made use of of the SIMBAD database, operated at CDS, Strasbourg, France.

REFERENCES

Alexander, D. R., & Ferguson, J. W. 1994, ApJ, 437, 879
Andersson, B.-G., Warnier, P. G., & Morris, M. 1991, ApJ, 366, 464
Augereau, J. C., Lagrange, A. M., Mouillet, D., & Ménard, F. 2001, A&A, 365, 78
Avedisova, V. 2000, Baltic Astron., 9, 569
Balona, L. A. 1994, MNRAS, 268, 119
Beskrovnaya, N. G., et al. 1998, A&AS, 127, 243
Böhm, T., & Catala, C. 1994, A&A, 290, 167
Böhm, T., & Hirth, G. A. 1997, A&A, 324, 177
Bouret, J.-C., & Catala, C. 1998, A&A, 340, 163

Carpenter, J. M., Snell, R. L., & Schloerb, F. P. 1995, ApJ, 450, 201
Castro-Carrizo, A., et al. 2002, A&A, 386, 633
Cohen, M., & Kuhi, L. V. 1979, ApJS, 41, 743
Corcoran, M., & Ray, T. P. 1997, A&A, 321, 189
———. 1998, A&A, 331, 147
Corradi, W. J. B., Franco, G. A. P., & Knude, J. 1997, A&A, 326, 1215
Courtès, G., Georgelin, Y. P., Georgelin, Y. M., & Monnet, G. 1970, in IAU Symp. 38, The Spiral Structure of our Galaxy, ed. W. Becker & G. I. Kontopoulos (Dordrecht: Reidel), 209
Dame, T. M., & Thaddeus, P. 1985, ApJ, 297, 751
Dame, T. M., et al. 1987, ApJ, 322, 706
Dambis, A. K., Mel'nick, A. M., & Rastorguev, A. S. 2001, Astron. Lett., 27, 58
de Jager, C., & Nieuwenhuijzen, H. 1987, A&A, 177, 217
de Winter, D., et al. 1999, A&A, 343, 137
de Zeeuw, P. T., et al. 1999, AJ, 117, 354
Duncan, A. R., Stewart, R. T., Haynes, R. F., & Jones, K. L. 1996, MNRAS, 280, 252
Eggen, O. J. 1978, PASP, 90, 436
Eiroa, C. 1991, ESO Sci. Rep., 11, 197
Feinstein, A. 1995, Rev. Mexicana Astron. Astrofis., 2, 57
Feitzinger, J. V., & Stuwe, J. A. 1984, A&AS, 58, 365 (erratum: 1986, A&AS63, 203)
———. 1986, ApJ, 305, 534
Finkenzeller, U. 1985, A&A, 151, 340
Finkenzeller, U., & Mundt, R. 1984, A&AS, 55, 109
Franco, G. A. P. 1989, A&A, 215, 119
———. 1990, A&A, 227, 499
García-Hernández, D. A., et al. 2002, A&A, 387, 955
Garcia-Lario, P., et al. 1993, A&A, 267, L11
———. 1997, A&AS, 126, 479
Graham, J. A. 1982, PASP, 94, 244
Gray, D. F. 1992, The Observation and Analysis of Stellar Photospheres (2d ed.; New York: Cambridge Univ. Press)
Gregorio-Hetem, J., & Hetem, A., Jr. 2002, MNRAS, 336, 197
Gregorio-Hetem, J., Sanzovo, G. C., & Lépine, J. R. D. 1988, A&AS, 76, 347
Gregorio-Hetem, J., et al. 1992, AJ, 103, 549
Grinin, V. P., et al. 1994, A&A, 292, 165
Hartley, M., et al. 1986, A&AS, 63, 27
Haug, U. 1970, A&AS, 1, 35
Haug, U., & Bredow, K. 1977, A&AS, 30, 235
Haug, U., Pfleiderer, J., & Dachs, J. 1966, Z. Astrophys., 64, 140
Herbig, G. H. 1960, ApJS, 4, 337
———. 1991, ESO Sci. Rep., 11, 59
Herbig, G. H., & Bell, K. R. 1995, Lick Obs. Bull., 1111, 5073
Herbst, W., & Racine, R. 1976, AJ, 81, 840
Higdon, J. C., & Lingenfelter, R. E. 1996, A&AS, 120, 349
Hillenbrand, L. A., et al. 1992, ApJ, 397, 613
Hilton, J., & Lahulla, J. F. 1995, A&AS, 113, 325
Iglesias, C. A., & Rogers, F. J. 1993, ApJ, 412, 752
Imhoff, C. L. 1994, in ASP Conf. Ser. 62, The Nature and Evolutionary Status of Herbig Ae/Be Stars, ed. P. S. Thé, M. R. Pérez, & E. P. J. van den Heuvel (San Francisco: ASP), 107
Jablonsky, F., Baptista, R., Barroso, F., Jr., Gneiding, C., Rodrigues, F., & Campos, R. P. 1994, PASP, 106, 1172
Kaltcheva, N. T., & Hilditch, R. W. 2000, MNRAS, 312, 753
Kenyon, S. J., & Hartmann, L. 1995, ApJS, 101, 117
Keto, E. R., & Myers, P. C. 1986, ApJ, 304, 466
Knude, J. 1984, in IAU Colloq. 81, Local Interstellar Medium, ed. Y. Kondo, F. C. Bruhweiler, B. D. Savage (Washington: NASA), 149
Knude, J., & Høg, E. 1998, A&A, 338, 897
Lizeau, R., Lorenzetti, D., Nisini, B., Spinoglio, L., & Moneti, A. 1992, A&A, 265, 577
Lynds, B. T. 1962, ApJS, 7, 1
Maddalena, R. J., & Thaddeus, P. 1985, ApJ, 294, 231
Maddalena, R. J., Morris, M., Moscowitz, J., & Thaddeus, P. 1986, ApJ, 303, 375
Magnani, L., Blitz, L., & Mundy, L. 1985, ApJ, 295, 402
Malfait, K., Bogaert, E., & Waelkens, C. 1998, A&A, 331, 211
Marraco, H. G., & Rydgren, A. E. 1981, AJ, 86, 62
Mazzitelli, I. 1989, ApJ, 340, 249
Mazzitelli, I., D'Antona, F., & Caloi, V. 1995, A&A, 302, 382
Miroshnichenko, A. S., et al. 1999, A&A, 347, 137
Mouillet, D., Lagrange, A. M., Augereau, J. C., & Ménard, F. 2001, A&A, 372, L61
Murdin, P., & Penston, M. V. 1977, MNRAS, 181, 657
Myers, P. C. 1975, ApJ, 198, 331
Parker, N. D. 1991, MNRAS, 251, 63
Persi, P., Polcaro, V. F., Viotti, R., & Origlia, L. 1991, MNRAS, 251, P1
Pettersson, B. 1991, ESO Sci. Rep., 11, 69
Piétu, V., Dutrey, A., & Kahane, C. 2003, A&A, 398, 565
Piskunov, N. E., Kupka, F., Ryabchikova, T. A., Weiss, W. W., & Jeffery, C. S. 1995, A&AS, 112, 525
Racine, R. 1968, AJ, 73, 233
Reipurth, B., Pedrosa, A., & Lago, M. T. V. T. 1996, A&AS, 120, 229
Schmidt-Kaler, T. 1982, in Landolt-Börnstein, Group VI, Volume 2, ed. K.-H. Hellwege (New York: Springer), 454
Shevchenko, V. S. 1999, Astron. Rep., 43, 246
Strafella, F., Pezzuto, S., Corciulo, G. G., Bianchini, A., & Vittone, A. A. 1998, ApJ, 505, 299
Tachirara, K., Dobashi, K., Mizuno, A., Okawa, H., & Fukui, Y. 1996, PASJ, 48, 489
Telting, J. H., Heemskerk, M. H. M., & Henrichs, H. F., & Savonije, G. J. 1994, A&A, 288, 558
Thé, P. S., de Winter, D., & Pérez, M. R. 1994, A&AS, 104, 315
Torres, C. A. O. 1999, Special Publ. 10 (Rio de Janeiro: Obs. Nac.)
Torres, C. A. O., et al. 1995, AJ, 109, 2146
Turner, D. G. 1976, ApJ, 210, 65
Ungerechts, H., & Thaddeus, P. 1987, ApJS, 63, 645
Valenti, J. A. 1994, Ph.D. thesis, Univ. California, Berkeley
Valenti, J. A., & Piskunov, N. 1996, A&AS, 118, 595
van den Ancker, M. E., de Winter, D., & Tjin, A., & Djie, H. R. E. 1998, A&A, 330, 145
Ventura, P., Zeppieri, A., Mazzitelli, I., & D'Antona, F. 1998, A&A, 334, 953
Vieira, S. L. A., Pogodin, M. A., & Franco, G. A. P. 1999, A&A, 345, 559
Whittet, D. C. B., et al. 1997, A&A, 327, 1194
Wouterloot, J. G. A., & Brand, J. 1989, A&AS, 80, 149
Yonekura, Y., et al. 1999, PASJ, 51, 837